

Band topology and non-trivial surface States in type-II Dirac semi-metal X(Ni, Pd)Te₂

N. K. Karn^{1,2*} and V.P.S. Awana^{1,2}

¹Academy of Scientific & Innovative Research (AcSIR), Ghaziabad, 201002, India

²CSIR- National Physical Laboratory, New Delhi, 110012, India

Abstract:

The semi-metals having electrons near the Fermi level follow the relativistic equation of motion, and show Dirac or Weyl-type behavior. Their orbital resolved electronic bands analysis indicates the non-trivial topological states. Through the first principle methods, the electronic band structure of bulk and thin layers of transition metal dichalcogenides NiTe₂ and PdTe₂ are calculated and analyzed. Implementation of Hubbard corrections to the band structure indicates zero magnetization, though atoms of Ni are magnetic. Z₂ invariant index is calculated for topological classification for both materials and is found to possess strong topology indicating robust topological surface states. Further, Fermi surfaces and topological surface states are computed into k_z plane showing the presence of Dirac-fermions by forming of Dirac cone for PdTe₂ but for NiTe₂ we do not get clear evidence.

Keywords: Dirac Semimetal, Density Functional Theory, Z₂ invariant, topological surface state.

*Corresponding Author

Navneet kumar Karn: E-mail: nkk15ms097@gmail.com

Senior Research Fellow

CSIR-NPL, New Delhi, India, 110060

Ph. +91-11-45609357

Introduction:

In the past decade, the quest for quantum materials with novel properties have been on a high and continues till today. Among these, materials with topological properties are mostly studied [1-4]. Topological insulators have a bulk bandgap; however, the gap is nonequivalent to traditional insulator vacuum due to surface state bands [5]. Apart from topological insulators, topological semimetals(TSM) has drawn the attention of condensed matter physicist as it provides an alternate platform to study the relativistic Dirac fermions [1, 3-5]. TSMs possess not only conducting non-trivial topological surface states but their bulk is also conducting, unlike the topological insulators. The semi-metals having electrons near the Fermi level follow a relativistic equation of motion, and show Dirac or Weyl-type behavior depending on the degeneracy of bands [6, 7].

Among various TSMs, the Transition Metal Dichalcogenides(TMD) are of special interest, as it is a 2-D layered material in which atomic layers are separated by a Vander Waals

gap. This makes them a good candidate for material intercalation [7, 8]. TMDs like PtTe₂ [9], PtSe₂ [10], PdTe₂ [8,11-14], and NiTe₂ [15-19] are considered to be type-II Dirac semimetal. Among these, PdTe₂ is found to be superconducting at 1.7K [20], by Au intercalation the T_c can be increased up to 4.7K [8]. Topological property with superconductivity makes PdTe₂ a potential material to realize topological superconductivity. The observed MR in these TMDs is not linear and is found to increase in a quadratic manner [14, 15]. The band structure analysis of these TMDs reveal that the Dirac point in these materials lies far below the Fermi level [12, 16, 18]. So, the transport in these materials is dominated by non-relativistic carriers. The Ni and Pd counterpart of these materials, such as NiTe₂ and PdTe₂ has been extensively studied in the context of topological properties [11-19]. These intrinsic noble characteristics of TSMs, including the topological superconductivity and non-linear MR, increase the eagerness to study the surface states.

Topological materials are characterized based on the symmetry they possess and associated invariants to that symmetry. For systems respecting time-reversal symmetry, the topology is characterized by Z₂ invariant index. There have been only a few scattered reports of Z₂ of these two TMD [16]. However, here for the first time we provide a topological classification of the two TMDs in terms of Z₂ invariant calculated by Wannier Charge Center (WCC) method. We report, both TMDs show strong topological character, with non-trivial surface states. Also, the surface states are calculated from the iterative greens function method from the different planes (110). The structure of these two TMDs is generated in VESTA [21] and we report the simulated XRD peaks of the same. To incorporate the van der Waal interaction between the 2D layers of the two TMDs, DFT-d3 corrections are implemented.

Computational Methods:

All computational simulation is performed on open-source software Quantum Espresso [22, 23] which works on the first principle-based DFT. The crystal structure is optimized and self-consistent functional calculations (SCF) have been performed to obtain the ground-state electron density and wavefunction. The electronic exchange and correlation corrections are incorporated by using the Perdew-Burke-Ernzerhof (PBE) type generalized gradient approximation (GGA) functionals [24]. The wave functions were expanded in a plane wave with a charge cut-off of 360 units and wave function cut-off of 45 Ry on a Monkhorst-Pack k-grid of 13×13×8. This computation produces the bulk electronic band structure and projected Density of states (PDOS) of both TMDs. To find any effect of magnetism on bands, DFT+U (Hubbard correction) calculations are implemented. Further, the Bloch wave functions generated by DFT are wannierized using WANNIER90 software [25] which produces maximally localized Wannier functions (MLWFs). The electronic band structure is recalculated using MLWFs and matched with the result obtained by the direct DFT method to check the quality of obtained MLWFs. Moreover, an effective tight-binding model is obtained based on these MLWFs for the material under investigation. For topological properties and calculation of Z₂ invariant, the tight-binding model is post-processed in the software WANNIER TOOLS [26]. The Wannier charge centers (WCC) are obtained of whose evolution in Brillouin zone planes indicated the states of Z₂-invariant. The surface spectral function was calculated using the iterative surface Green's function method [27, 28] along the (001) plane.

Results and Discussion:

Both compounds under investigation PdTe₂ and NiTe₂ crystallize in trigonal with the P-3m1(164) space group which belongs to centrosymmetric space groups. The structure is a 2D layered structure, which is separated by Van Der Waal's gap. The Waykoff position of the

atoms X(Ni, Pd) is 1a (0, 0, 0) and Te atoms at 2d (0.33, 0.66, 0.25). The structure generated using VESTA software is shown in fig. 1(a) and 1(b). Cell parameters of the NiTe₂ unit cell are $a = b = 3.855 \text{ \AA}$ & $c = 5.277 \text{ \AA}$, $\alpha = \beta = 90.0$, and $\gamma = 120.0$; and the same of PdTe₂ are $a = b = 7.631 \text{ \AA}$ & $c = 9.717 \text{ \AA}$, $\alpha = \beta = 90.0$ and $\gamma = 120$. Theoretically, XRD patterns are also calculated using VESTA as shown in figure 1(c) confirming the used phase in the calculation is correct. The XRD peaks also match with the reported XRD peaks of NiTe₂ [29] and PdTe₂ [14].

Band Structure:

The theoretical calculation is performed using the DFT-based software Quantum espresso. The high symmetric path in the first Brillouin zone(BZ) is chosen for band structure calculation as shown in the inset of fig1(c). This is the optimized path suggested by the work of Hinuma et. al. [30]. Since both materials belong to the same crystal class, their first BZ is similar having the same high symmetric points. The suggested path is A-H-L-A- Γ -M-K- Γ . The calculated band structure of NiTe₂ is shown in fig. 2(a) where as for PdTe₂ the same is shown in figure 2(d). It has been found that higher levels of theory, such as DFT-D3 [31], MP2 [32], and B3LYP[33], give more accurate results. Since the crystal under study has van der Waals gaps between its layers, we also included the van der Waals correction, for which DFT-D3 calculation was performed [31]. The dispersion correction energy was evaluated as -0.83 eV . Both TMDs show very similar band structure features. In both cases, without SOC bands show a double degenerate Dirac-cone in between the path L-A around 0.5eV above the Fermi energy. However, when SOC parameters are included the band degeneracy is lifted. Another triply degenerate point is observable along path A- Γ which decomposes into one four-fold degenerate point and a doubly degenerate band. Fig. 2(b) and (e) show the orbital projected density of states (PDOS) without SOC while figs 2(c) and (f) show the PDOS when SOC is included. From the PDOS, we know the orbital contributions for the bands near the Fermi level. In both cases, the d orbital of transition metal and the p orbital of Te atoms. The total DOS near the Fermi level is finite, which confirms the semi-metallic nature of both TMDs. Also, note that the Dirac cone is classified as type I or II based on its tilt. Here in the band structure, both Dirac cones above discussed are tilted, therefore both TMDs are regarded as type-II Dirac semimetals.

It is well known that Ni has a magnetic moment, so we performed magnetization calculations including the Hubbard corrections. We observe that the net magnetization is zero for both TMDs. Therefore, the implementation of Hubbard corrections to the band structure does not alter the electronic band structure. This implies that Ni atoms in the unit cell have opposite magnetization i.e. atoms are in an antiferromagnetic state. Thus we have a non-magnetic system. The system respects the time-reversal symmetry(TRS) which is confirmed through the SOC band structure calculation. If TRS is not followed, the double degeneracy would have been lifted but here each band is doubly degenerate.

Further, to compute Z₂ invariant and surface states, the wavefunctions from first principle calculations are wannierized and the band analysis confirms the orbital contributions for the near Fermi-level bands. From these wannierized we have constructed tight-binding Hamiltonian and implemented it in Wannier Tools. Using the iterative Green's function methods, the surface state spectrum of the two TMDs is calculated. The surface card is set to be in the plane (110), and the calculation was done by taking 81 slices of one reciprocal vector. The path taken for surface state spectrum calculation is $K \rightarrow \Gamma \rightarrow K$.

The surface state spectrum of NiTe₂ is shown in fig. 3(a) and the same of PdTe₂ is shown in fig. 3(b). We observe that the Dirac cone is present at the Γ point around 0.5 eV above the Fermi level in the case of PdTe₂. However, the same feature is not sharply present in the case of NiTe₂. Thus, the computational simulation indicates the presence of surface states in the 110 planes in PdTe₂ but the same is not clearly evidenced in the case of NiTe₂. In the next section, the calculation of the Z₂ invariant confirms that both are equally likely to possess a non-trivial topological surface state.

Z₂ – invariant:

Based on the symmetry principle, there are several topological invariants to classify the topology present in the system. For the systems respecting TRS, Z₂ invariant [34]; for TRS broken phase chern number; for crystals with reflection symmetry mirror chern number [35]; for topological magnetic phases, Z₄ [36] are some of the topological invariants following the symmetry present in the crystal. Here, we find that the TMDs under study are non-magnetic and respect TRS, so the Z₂ invariant is to be computed for its topological classification. Different Z₂-states are separated by a topological phase transition which involves an adiabatic transformation of the bands leading to the gap closing of the two bands. There are several methods to calculate Z₂ invariant - discrete method involves finding Pfaffians/parity over the fixed points of the time-reversal symmetry[34], Fukui- Hatsugai method [37], and by tracking the windings of the Wannier Charge Center (WCC) evolution around the BZ [38, 39]. Here, we use the WCC method to compute the Z₂ invariant which is incorporated into WANNIER TOOLS. The WCC evolved by changing the k vector, odd or even number of exchange of these charge centers in different k-planes, defining non-trivial or trivial topology respectively. So from the tight-binding model obtained for Wannier functions, the WCCs are computed numerically and evolved in the 6-planes – $k_x, k_y, k_z = 0$ and $k_x, k_y, k_z = 0.5$ in the Brillouin zone. An odd number of the crossing of WCC implies a topologically non-trivial state (Z₂=1), whereas an even number of crossings indicate the presence of a topologically trivial state (Z₂=0). The computed Z₂ invariants for both TMDs are shown in table 1.

For 3D systems, the Z₂ topological invariants are represented by four indices ($\nu_0; \nu_1 \nu_2 \nu_3$). These indices are calculated by the formula [38, 39]

$$\begin{aligned} \nu_0 &= \sum \text{of } Z_2 \in k_i \text{ plane mod } 2 \\ \nu_i &= Z_2 \text{ value} \in (k_i=0.5) \text{ plane} \end{aligned}$$

where $i=x,y,z$. The first index designates a strong topology and the rest three indices indicate a weak topology present in the system. Without SOC bands we encounter degeneracies but with SOC bands we do not encounter any band degeneracy. This allows us to compute the Z₂ invariant for SOC bands. From Table 1, following the above method, we get the Z₂ index for both TMDs as (1; 000) which is exactly the same as the previously well-established topological insulator Bi₂Te₃ [40] with a strong topological index. The weak topological index shows trivial states at the surfaces $k_i= 0.5$ for both TMDs. However, both TMDs demonstrate strong non-trivial topological phases with $\nu_0=1$. This gives clear evidence of band inversion when SOC comes into play as degeneracies are lifted. From the surface states calculation compared to the Z₂ invariant obtained we observe non-trivial topological surface states are more prominent in PdTe₂ compared to NiTe₂.

Conclusion:

To summarize, in the present work, through the first principle methods, the electronic band structure of bulk and thin layers of transition metal dichalcogenides NiTe₂ and PdTe₂ are calculated and analyzed. Both belong to the same class of compounds which crystallizes trigonal lattice with P-3m1(164) space group which is centrosymmetric. The projected density of states calculation confirms the semi-metallic nature as it turns out to be finite. This also shows the valance and conduction band near the Fermi level are mostly originating from the d orbital of transition metal and the p orbital of Te atoms. Magnetic calculation shows the net magnetic moment is zero for both systems though one contains highly magnetic Ni atoms. Therefore, the implementation of Hubbard corrections to the band structure does not alter the electronic band structure. The electronic band dispersion in k_z plane shows the formation of the Dirac cone at the center of k_z plane. With no magnetization, band structure analysis tells that the high symmetric point Γ is a time-reversal invariant momentum point. This allows us to calculate Z₂ invariant index for both systems for topological classification and is found to possess strong topology indicating robust topological surface states. Further, Fermi surfaces and topological surface states are computed into k_z plane of the reciprocal space showing the presence of Dirac - Fermion by the formation of Dirac cone for PdTe₂ but for NiTe₂ we do not get clear evidence.

Acknowledgment:

The authors would like to thank Director NPL for his keen interest and encouragement. N.K. Karn would like to thank CSIR for the research fellowship. N. K. Karn would also like to thank AcSIR for Ph.D. registration.

Conflict of Interest Statement:

The authors have no conflict of interest.

Figure Captions:

Figure 1: Trigonal unit cell of (a)NiTe₂ (b) PdTe₂ with space group P-3m1. (c)The simulated XRD peaks of the two TMDs. The inset figure shows the first Brillouin zone, with the Green arrows directing the path chosen for the Band structure calculation.

Figure 2: (a) The electronic band structure of NiTe₂ with and without SOC parameters including DFT-D3 corrections. (b) and (c) show the projected density of states without and with SOC respectively for NiTe₂. (d) Shows the electronic band structure of PdTe₂ with and without SOC parameters. (e) and (f) show the projected density of states without and with SOC respectively for PdTe₂.

Figure 3: This shows the surface state spectrum, (a) for NiTe₂ a band degeneracy is there at Γ but the Dirac cone is not apparent. (b) surface state spectrum PdTe₂. Dirac cone is observable at Γ point around energy 0.5 eV.

References

1. Wieder, B.J., Bradlyn, B., Cano, J. *et al.* Topological materials discovery from crystal symmetry. *Nat Rev Mater* **7**, 196–216 (2022).

2. Sharma, M. M., Sharma, P., Karn, N. K., & Awana, V. P. (2022). Comprehensive review on topological superconducting materials and interfaces. *Superconductor Science and Technology*, **35**(8), 083003 (2022).
3. Liu, J. A short review on first-principles study of gapped topological materials. *Computational Materials Science*, **195**, 110467 (2021).
4. Gao, H., Venderbos, J. W. F., Kim, Y., & Rappe, A. M. Topological semimetals from first principles. *Annual Review of Materials Research*, **49**(1), 153–183 (2019).
5. Hasan, M. Z., & Moore, J. E. Three-dimensional topological insulators. *Annual Review of Condensed Matter Physics*, **2**(1), 55–78 (2011).
6. Bradlyn, B., Cano, J., Wang, Z., Vergniory, M. G., Felser, C., Cava, R. J., & Bernevig, B. A. Beyond Dirac and Weyl fermions: Unconventional quasiparticles in conventional crystals. *Science*, **353**, 6299 (2016).
7. Rajapakse, M. et al. Intercalation as a versatile tool for fabrication, property tuning, and phase transitions in 2D materials. *Npj 2D Materials and Applications*, **5**(1) (2021).
8. Kudo, K., Ishii, H., & Nohara, M. Composition-induced structural instability and strong-coupling superconductivity in $\text{Au}_{1-x}\text{Pd}_x\text{Te}_2$. *Physical Review B*, **93**(14) (2016).
9. Zheng, W. et al. Detailed study of the Fermi surfaces of the type-II dirac semimetallic candidates XTe_2 ($X=\text{Pd}, \text{Pt}$). *Physical Review B*, **97**(23) (2018).
10. Zhang, K. et al. Experimental evidence for type-II dirac semimetal in PtSe_2 . *Physical Review B*, **96**, 12 (2017).
11. Fei, F. et al. Nontrivial Berry phase and type-II dirac transport in the layered material PdTe_2 . *Physical Review B*, **96**(4) (2017).
12. Liu, Y. et al. Identification of topological surface state in PdTe_2 superconductor by angle-resolved photoemission spectroscopy. *Chinese Physics Letters*, **32**(6), 067303 (2015).
13. Liu, C. et al. Two-dimensional superconductivity and topological states in PdTe_2 thin films. *Physical Review Materials*, **2**(9) (2018).
14. Kumar, Y., Sharma, P., Sharma, M.M. et al. Investigation of structural and magnetotransport properties of PdTe_2 single crystals. *Appl. Phys. A* **128**, 880 (2022).
15. Kar, I., & Thirupathiah, S. (2022). Crossover from linear to quadratic magnetoresistance in NiTe_2 . *Materials Today: Proceedings*, **65**, 70-73.
16. Ghosh, B. et al. Observation of bulk states and spin-polarized topological surface states in transition metal dichalcogenide Dirac semimetal candidate NiTe_2 . *Physical Review B*, **100**(19) (2019).
17. Xu, C. et al. Topological type-II Dirac fermions approaching the Fermi level in a transition metal dichalcogenide NiTe_2 . *Chemistry of Materials*, **30**(14), 4823-4830 (2018).
18. Hlevyack, J. A. et al. Dimensional crossover and band topology evolution in Ultrathin semimetallic NiTe_2 films. *Npj 2D Materials and Applications*, **5**(1) (2021).
19. Mukherjee, S. et al. Fermi-crossing type-II dirac fermions and topological surface states in NiTe_2 . *Scientific Reports*, **10**(1) (2020).
20. Amit, & Singh, Y. Heat capacity evidence for conventional superconductivity in the type-II dirac semimetal PdTe_2 . *Physical Review B*, **97**(5) (2018).
21. Momma, K., & Izumi, F. VESTA 3 for three-dimensional visualization of crystal, volumetric and morphology data. *Journal of Applied Crystallography*, **44**(6), 1272–1276 (2011).
22. Giannozzi, P. et al. Quantum Espresso: A modular and open-source software project for quantum simulations of materials. *Journal of Physics: Condensed Matter*, **21**(39), 395502 (2009).

23. Giannozzi, P. et al.(2017). Advanced capabilities for materials modelling with Quantum Espresso. *Journal of Physics: Condensed Matter*, **29**(46), 465901 (2009).
24. Perdew, J. P., Burke, K., & Ernzerhof, M. . Generalized gradient approximation made simple. *Physical Review Letters*, **77**(18), 3865–3868 (1996).
25. Mostofi, A. A., Yates, J. R., Pizzi, G., Lee, Y.-S., Souza, I., Vanderbilt, D., & Marzari, N. (2014). An updated version of WANNIER90: A tool for obtaining maximally-localised Wannier functions. *Computer Physics Communications*, **185**(8), 2309–2310.
26. Wu, Q. S., Zhang, S. N., Song, H.-F., Troyer, M., & Soluyanov, A. A. (2018). WannierTools: An open-source software package for novel topological materials. *Computer Physics Communications*, **224**, 405–416.
27. Sancho, M. P., Sancho, J. M., & Rubio, J. Quick Iterative Scheme for the calculation of transfer matrices: Application to mo (100). *Journal of Physics F: Metal Physics*, **14**(5), 1205-1215 (1984).
28. Sancho, M. P., Sancho, J. M., Sancho, J. M., & Rubio, J. Highly convergent schemes for the calculation of bulk and Surface Green functions. *Journal of Physics F: Metal Physics*, **15**(4), 851-858 (1985).
29. Guo, J., Shi, Y., Chu, Y., & Ma, T. Highly efficient telluride electrocatalysts for use as PT-free counter electrodes in dye-sensitized solar cells. *Chemical Communications*, **49**(86), 10157 (2013).
30. Hinuma, Y., Pizzi, G., Kumagai, Y., Oba, F., & Tanaka, I. Band structure diagram paths based on Crystallography. *Computational Materials Science*, **128**, 140-184 (2017).
31. Grimme, S., Antony, J., Ehrlich, S., & Krieg, H. A consistent and accurate *ab initio* parametrization of density functional dispersion correction (DFT-D) for the 94 elements H-Pu. *The Journal of Chemical Physics*, **132**(15), 154104 (2010)..
32. Møller C., Plesset M.S. Note on an approximation treatment for many-electron systems. *Phys Rev.*, **46**, 618–622 (1934).
33. Stephens, P. J., Devlin, F. J., Chabalowski, C. F., & Frisch, M. J. Ab initio calculation of vibrational absorption and circular dichroism spectra using density functional force fields. *The Journal of Physical Chemistry*, **98**(45), 11623-11627 (1994).
34. Fu, L., & Kane, C. L. Topological insulators with inversion symmetry. *Physical Review B*, **76**(4) (2007).
35. Hsieh, T. H., Lin, H., Liu, J., Duan, W., Bansil, A., & Fu, L. Topological crystalline insulators in the SnTe material class. *Nature Communications*, **3**(1) (2012).
36. Tanaka, Y., Takahashi, R., Zhang, T., & Murakami, S. Theory of inversion-z4 protected topological chiral hinge states and its applications to layered antiferromagnets. *Physical Review Research*, **2**(4) (2020).
37. Fukui, T., & Hatsugai, Y. Quantum Spin Hall effect in three dimensional materials: Lattice computation of Z2 topological invariants and its application to Bi and Sb. *Journal of the Physical Society of Japan*, **76**(5), 053702 (2007).
38. Soluyanov, A. A., & Vanderbilt, D. Computing topological invariants without inversion symmetry. *Physical Review B*, **83**(23) (2011).
39. Yu, R., Qi, X. L., Bernevig, A., Fang, Z., & Dai, X. Equivalent expression of z2 topological invariant for band insulators using the non-abelian berry connection. *Physical Review B*, **84**(7) (2011).
40. Rauch, T., Flieger, M., Henk, J., Mertig, I., & Ernst, A. Dual topological character of chalcogenides: Theory for Bi2Te3. *Physical Review Letters*, **112**(1) (2014).

Figures:

Figure 1.

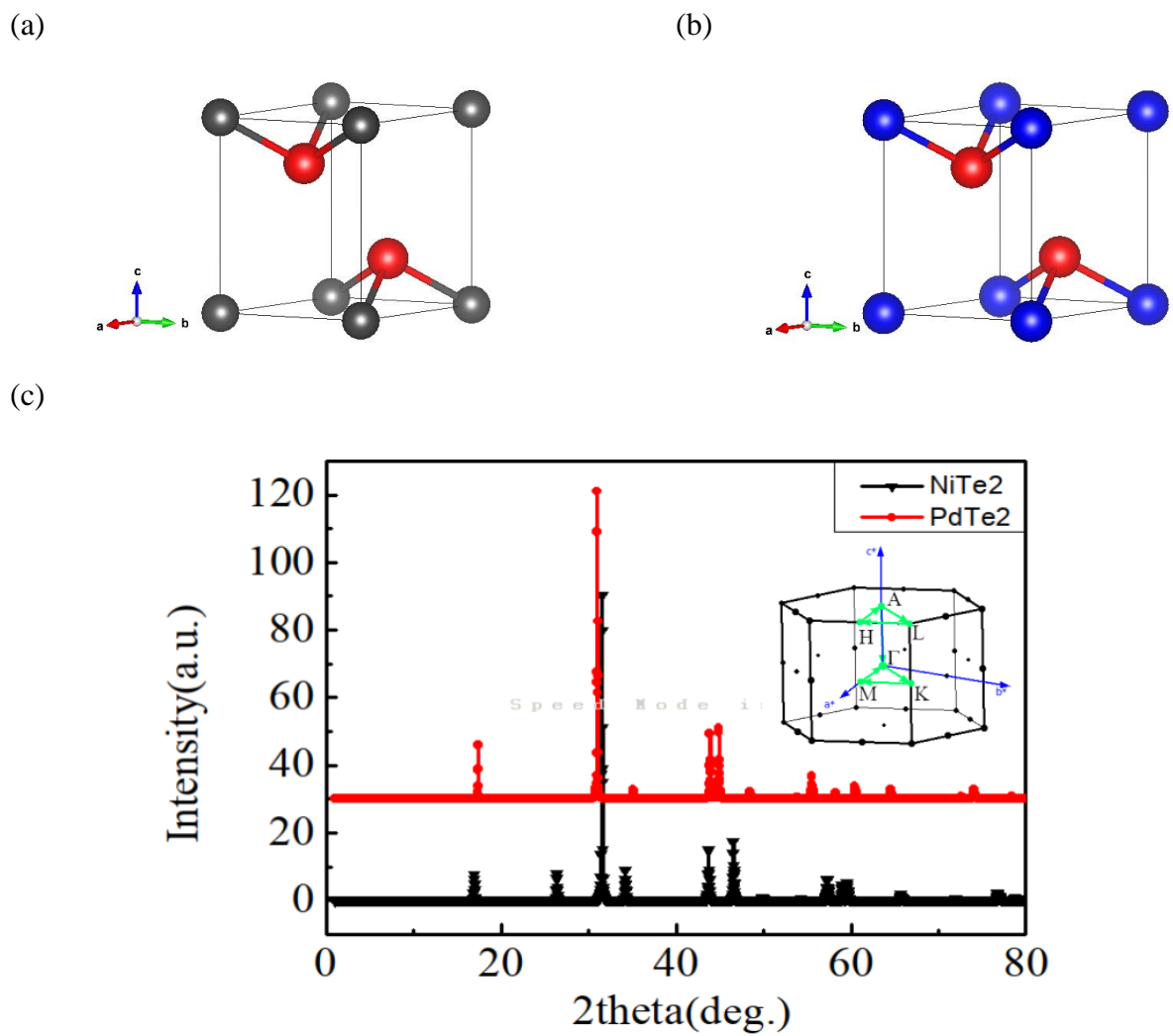
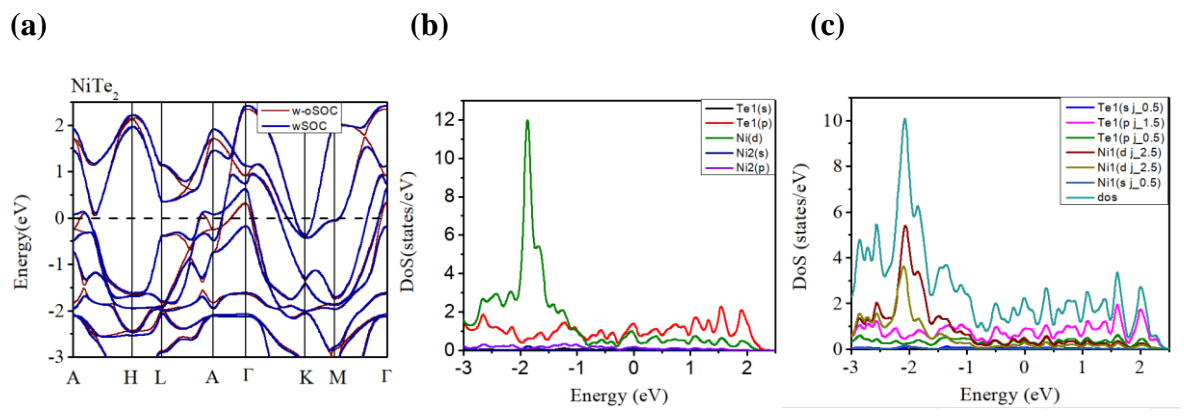


Figure 2



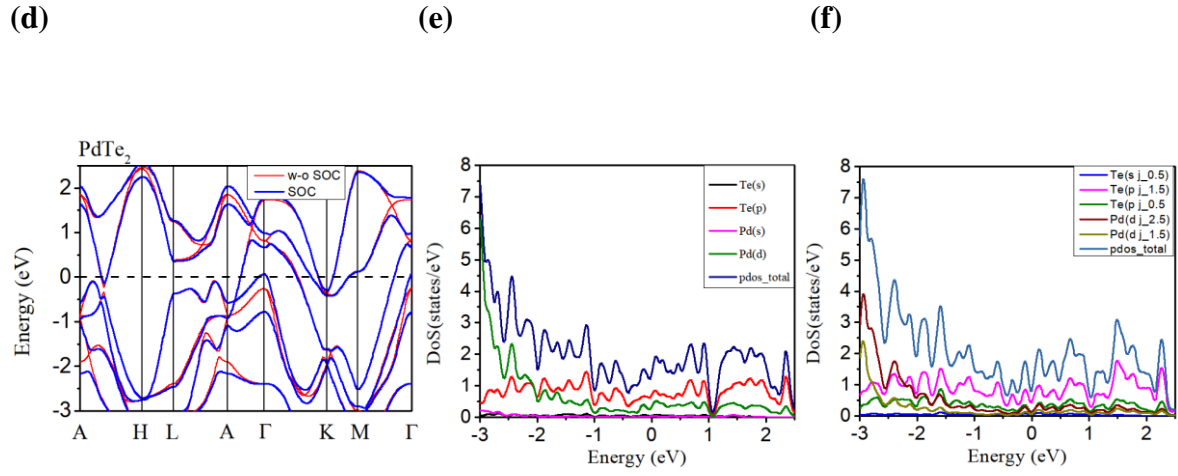


Figure 3.

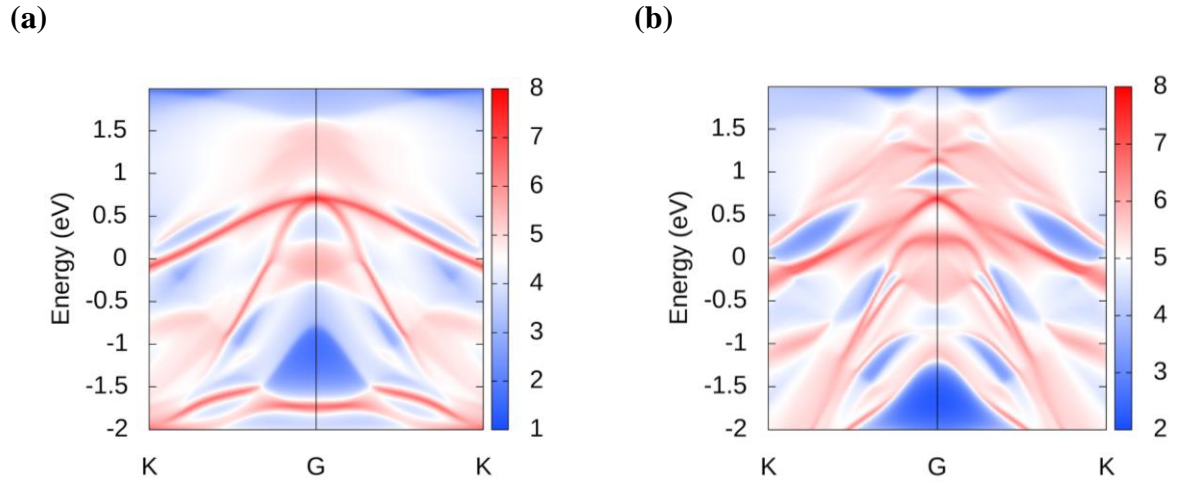


Table 1

Z2 invariant

Plane	NiTe ₂	PdTe ₂
$k_x = 0.0, k_y$ - k_z plane	1	1
$k_x = 0.0, k_y$ - k_z plane	0	0
$k_x = 0.0, k_y$ - k_z plane	1	1
$k_x = 0.0, k_y$ - k_z plane	0	0
$k_x = 0.0, k_y$ - k_z plane	1	1
$k_x = 0.0, k_y$ - k_z plane	0	0